Available online at www.sciencedirect.com
SCIENCE DIRECT®
ELSEVIER
International Journal of Solids and Structures 43 (2006) 172–192
INTERNATIONAL JOURNAL OF SOLIDS and STRUCTURES
www.elsevier.com/locate/ijsolstr

Topological shape optimization of power flow problems at high frequencies using level set approach

Seonho Cho *, Seung-Hyun Ha, Chan-Young Park

Department of Naval Architecture and Ocean Engineering, Seoul National University, San 56-1, Sillim-Dong, Kwanak-Gu, Seoul, Republic of Korea

Received 16 August 2004
Available online 8 June 2005

Abstract

Using a level set method we develop a topological shape optimization method applied to power flow problems in steady state. Necessary design gradients are computed using an efficient adjoint sensitivity analysis method. The boundaries are implicitly represented by the level set function obtainable from the ''Hamilton–Jacobi type'' equation with the ''Up-wind scheme.'' The implicit function is embedded into a fixed initial domain to obtain the finite element response and sensitivity. The developed method defines a Lagrangian function for the constrained optimization. It minimizes a generalized compliance, satisfying the constraint of allowable volume through the variations of implicit boundary. During the optimization, the boundary velocity to integrate the Hamilton–Jacobi equation is obtained from the optimality condition for the Lagrangian function. Compared with the established topology optimization method, the developed one has no numerical instability such as checkerboard problems and easy representation of topological shape variations.

Keywords: Topological shape optimization; Power flow problem; Level set method; Hamilton–Jacobi equation; Adjoint variable method

1. Introduction

For the dynamic analysis of structural systems in high frequency range, the finite element method (FEM) and boundary element method (BEM) to obtain the kinematic responses are not suitable due to the requirement of mesh size that is closely related to the quality of analysis. Moreover, at high frequencies,

* Corresponding author. Tel.: +82 2 880 7322; fax: +82 2 888 9298.
E-mail address: secho@snu.ac.kr (S. Cho).

0020-7683/$ - see front matter © 2005 Elsevier Ltd. All rights reserved.
doi:10.1016/j.ijsolstr.2005.04.033

the uncertainty of system parameters gets increased and consequently the quality of analysis results becomes worse. Therefore, it is desirable to employ the statistical methods that predict the modal- and frequency-averaged vibrational behavior of systems. Statistical energy analysis (SEA) is one of the methods developed to overcome the difficulties in high frequency ranges. However, the SEA is well suited only for high frequency problems with high modal density. Also it does not provide the spatial information of energy distribution. Another alternative is a power flow analysis (PFA) method. The PFA method regards "flow of vibrational energy" as "flow of heat" in thermal systems. Similar to the thermal problems, the governing equation for the PFA is a parabolic partial differential equation. The PFA enables to predict the spatial energy variation in structures and handle local damping. The PFA is originally devised by Belov et al. (1977). Butlitskaya et al. (1983) used the energy equation developed by Belov et al. to investigate the propagation of both vibrational and acoustic energy in structures. Recently, Nefske and Sung (1989) performed a finite element implementation of vibrational energy equation. The developed power flow finite element method (PFFEM) is used to predict the vibrational response of beams excited by point harmonic forces.

Topology optimization methods enable designers to find a suitable structural layout for required system performances. Ever since Bendsøe and Kikuchi (1988) introduced the topology optimization using a homogenization method, many topology optimization methods have been developed for both linear and nonlinear structural problems in many disciplines such as solid mechanics, thermal, eigenvalue, and acoustic problems. Nowadays, the density method (Bendsøe, 1989) is preferred due to its simple implementation compared with the homogenization method. This method defines a bulk material density, regarded as the design variable varying from zero (void state) to unity (solid state), to distribute the material in the continuum design domain. In the level set approach for the topology optimization, keeping the material homogeneous in the domain, its boundary rather than the material distribution is varying to meet the optimization requirements. Furthermore, there is no need to consider the checkerboard patterns of material distribution which is one of the frequently encountered numerical instabilities in the established topology optimization methods.

Since the topology optimization necessarily involves many design variables, the sensitivity of performance measures with respect to the design variables should be determined in a very efficient way. The adjoint variable method (AVM) is computationally efficient especially for the problems that have many design variables but small number of performance measures because their design sensitivity can be computed in a selective manner (Haug et al., 1986). Thus it is widely used in the topology optimization problems. In this paper, a continuum method for the boundary variations is considered. Recently, Kim et al. (2004) developed an efficient DSA method for the power flow problems in steady state.

Osher and Sethian (1988) have devised a level set method for numerically tracking fronts and free boundaries, which is used in many applications as motion by mean curvature. Sethian and Wiegmann (2000) discussed about the resolution of the boundaries. In their paper, an explicit jump immersed interface method is employed to compute the response of two-dimensional linear elasto-static problems of complex geometries without meshes. Also, they use the material removal and addition scheme. The removal rate determines the closed stress contours along the new holes and the velocity of the boundary motion. Allaire et al. (2002) described a new implementation of a level set method for shape optimization. In their formulation, the compliance and target displacement objectives are considered. The algorithm creates no holes inside the domain and converges to a local minimum which strongly depends on the initial topology. Wang et al. (2003) developed a numerical procedure for topology optimization using an implicit moving boundary. They represent the structural boundary using the level set model that is embedded in a higher dimensional scalar function.

In Section 2, the governing equation and weak formulation for the power flow problems are discussed. In Section 3, after defining a level set function and solving the "Hamilton–Jacobi" equation, the implicit moving boundary is embedded in the weak formulation. In Section 4, we formulate a topological shape

optimization for the power flow problems using the adjoint sensitivity and a gradient-based optimization method. In Section 5, some demonstrative numerical examples for various cases are presented, which show similar results in comparison with the established topology optimization method.

2. Power flow problems

Consider a structural body occupying an open domain Ω bounded by a closed surface Γ as shown in Fig. 1. All the material properties are assumed homogeneous and isotropic in the domain Ω.

Boundaries are composed of an energy boundary Γ^e and a flux boundary Γ^q such that

$$\Gamma^e \cup \Gamma^q = \Gamma \quad \text{and} \quad \Gamma^e \cap \Gamma^q = \phi. \tag{1}$$

The body is subjected to the rate of internal energy generation π and the following boundary conditions. A prescribed energy density e_0 on Γ^e and a prescribed energy flux q_0 on Γ^q in the inward normal direction are imposed. **n** is an outward unit vector normal to the boundary.

For an energy field e, the governing equation for the power flow problems in steady state is written by

$$-\frac{c_g^2}{\eta\omega}\nabla^2 e + \eta\omega e = \pi, \tag{2}$$

where e, η, ω, and c_g are the time- and space-averaged energy density function, hysteresis damping factor, exciting frequency, and group speed, respectively. For plate structures, the group velocity is defined by

$$c_g = 2 \cdot \sqrt[4]{\frac{\omega^2 D}{\rho h}} = 2 \cdot \sqrt[4]{\frac{\omega^2 E h^2}{12\rho(1-\nu^2)}}, \tag{3}$$

where ρ, ν, h, and D are the density, Poisson's ratio, thickness, and flexural rigidity of plate, respectively. The boundary conditions are applied as

$$e = e_0 \quad \text{on } \Gamma^e \tag{4}$$

and

$$q = q_0 \quad \text{on } \Gamma^q. \tag{5}$$

The space Z for the trial solution is defined by

$$Z = \{e \in [H^1(\Omega)]^d : e = e_0 \text{ on } \Gamma^e\}, \tag{6}$$

where d represents the dimension of problem and $H^1(\Omega)$ is the Hilbert space of order one. The space $\overline{Z}$ for the virtual field is defined by

$$\overline{Z} = \{\bar{e} \in [H^1(\Omega)]^d : \bar{e} = 0 \text{ on } \Gamma^e\}. \tag{7}$$

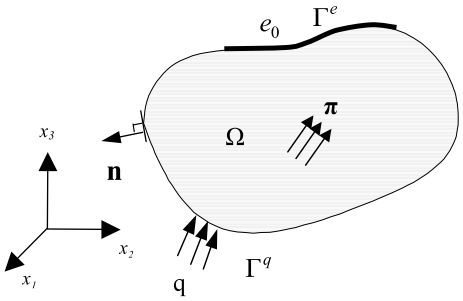

Fig. 1. Structural body in space.

Using the virtual field $\bar{e}$ that satisfies homogeneous Dirichlet boundary conditions, the weak form of Eq. (2) is written as

$$\int_{\Omega}\left(-\frac{c_{\mathrm{g}}^2}{\eta\omega}\nabla^2 e\bar{e}+\eta\omega e\bar{e}\right)\mathrm{d}\Omega=\int_{\Omega}\pi\bar{e}\,\mathrm{d}\Omega\quad\text{for all }\bar{e}\in\overline{Z}. \tag{8}$$

Using the divergence theorem, Eq. (8) can be rewritten as

$$\int_{\Omega}\left(\frac{c_{\mathrm{g}}^2}{\eta\omega}\nabla e\cdot\nabla\bar{e}+\eta\omega e\bar{e}\right)\mathrm{d}\Omega=\int_{\Omega}\pi\bar{e}\,\mathrm{d}\Omega-\int_{\Gamma^q}\left(-\frac{c_{\mathrm{g}}^2}{\eta\omega}\nabla e\right)\cdot\mathbf{n}\bar{e}\,\mathrm{d}\Gamma\quad\text{for all }\bar{e}\in\overline{Z}. \tag{9}$$

Defining a time- and space-averaged energy intensity $\mathbf{I}$ as

$$\mathbf{I}=-\frac{c_{\mathrm{g}}^2}{\eta\omega}\nabla e \tag{10}$$

and an energy flux q as

$$q=\mathbf{n}\cdot\mathbf{I}, \tag{11}$$

Eq. (9) is reduced to

$$\int_{\Omega}\left(\frac{c_{\mathrm{g}}^2}{\eta\omega}\nabla e\cdot\nabla\bar{e}+\eta\omega e\bar{e}\right)\mathrm{d}\Omega=\int_{\Omega}\pi\bar{e}\,\mathrm{d}\Omega-\int_{\Gamma^q}q\bar{e}\,\mathrm{d}\Gamma\quad\text{for all }\bar{e}\in\overline{Z}. \tag{12}$$

Defining a bilinear form

$$a(e,\bar{e})\equiv\int_{\Omega}\left(\frac{c_{\mathrm{g}}^2}{\eta\omega}\nabla e\cdot\nabla\bar{e}+\eta\omega e\bar{e}\right)\mathrm{d}\Omega \tag{13}$$

and a linear form

$$\ell(\bar{e})\equiv\int_{\Omega}\pi\bar{e}\,\mathrm{d}\Omega-\int_{\Gamma^q}q\bar{e}\,\mathrm{d}\Gamma. \tag{14}$$

Eq. (12) can be rewritten as

$$\text{Find } e\in Z \text{ such that } a(e,\bar{e})=\ell(\bar{e})\quad\text{for all }\bar{e}\in\overline{Z}. \tag{15}$$

3. Level set formulation

Let $\Omega\subset R^d$ be a bounded open domain with a smooth boundary Γ, at a generic configuration, (as shown in Fig. 2)

$$\Omega=\Omega_{\mathrm{N}}\cup\Omega_{\mathrm{D}}, \tag{16}$$

where Ω_{N} and Ω_{D} are a non-designable and a designable domains, respectively. The R^d stands for a d-dimensional real space. Imagine the boundary of domain Γ moves in the direction normal to its boundary with a known speed V_n. To derive the equation of moving boundary as time evolves, we embed this propagating boundary as the zero level set ϕ of a $(d+1)$-dimensional function $\Phi(\phi,k)$. Given a closed d-dimensional hyper-surface Γ at zero level, we come up with a formulation for the motion of the hyper-surface Γ_τ propagating along its normal direction with the speed V_n at time τ. Let Γ_{I} and Ω_{I} be an initial reference

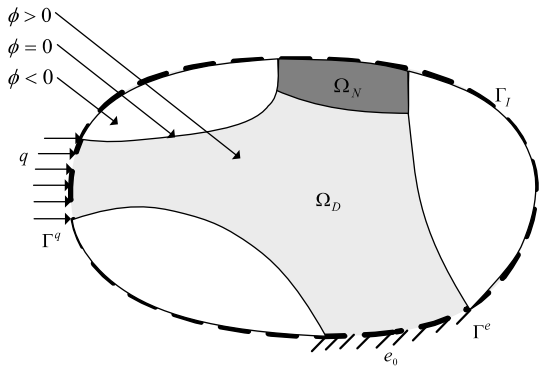

Fig. 2. Design domains and level set function.

boundary and domain, respectively. At time $\tau = 0$, assume the existence of a zero level set function $\phi(\mathbf{x}, 0)$ that is Lipschitz continuous and defined on Ω_{I}, satisfying

$$\phi(\mathbf{x}, \tau = 0)\begin{cases} +\zeta(\mathbf{x}, \Gamma) & \mathbf{x} \in \Omega, \\ = 0 & \mathbf{x} \in \Gamma, \\ -\zeta(\mathbf{x}, \Gamma) & \mathbf{x} \in \Omega_{\mathrm{I}} \backslash \overline{\Omega}, \end{cases} \tag{17}$$

where $\zeta(\mathbf{x}, \Gamma)$ is a distance from a point $\mathbf{x}$ to the boundary Γ, for all $\mathbf{x} \in R^d$. Also let Γ_τ and Ω_τ be a moving boundary and a corresponding domain at time τ, respectively. Define an evolving level set function $\phi(\mathbf{x}_\tau, \tau)$ that is Lipschitz continuous and also defined on Ω_{I}, satisfying

$$\phi(\mathbf{x}_\tau, \tau)\begin{cases} +\zeta(\mathbf{x}_\tau, \Gamma_\tau) & \mathbf{x}_\tau \in \Omega_\tau, \\ = 0 & \mathbf{x}_\tau \in \Gamma_\tau, \\ -\zeta(\mathbf{x}_\tau, \Gamma_\tau) & \mathbf{x}_\tau \in \Omega_{\mathrm{I}} \backslash \overline{\Omega}_\tau, \end{cases} \tag{18}$$

where Ω_{I} represents an initial reference domain that includes all the possible domains Ω_τ, i.e.

$$\Omega_\tau \subseteq \Omega_{\mathrm{I}}. \tag{19}$$

An outward unit vector $\mathbf{n}$ normal to the boundary Γ is obtained by

$$\mathbf{n} = -\frac{\nabla\phi}{|\nabla\phi|}. \tag{20}$$

A curvature κ is defined by the divergence of $\mathbf{n}$, as

$$\kappa = \operatorname{div}\mathbf{n} = -\nabla \cdot \left(\frac{\nabla\phi}{|\nabla\phi|}\right). \tag{21}$$

Also, the area and length of boundary are obtained, respectively, by

$$\mathrm{Area}(\Omega) = \int_{\Omega_{\mathrm{I}}} \hat{H}(\phi)\,\mathrm{d}\Omega \tag{22}$$

and

$$\mathrm{Length}(\Gamma) = \int_{\Omega_{\mathrm{I}}} \delta(\phi)|\nabla\phi|\,\mathrm{d}\Omega, \tag{23}$$

where $\hat{H}(x)$ and $\delta(x)$ are the Heaviside and Dirac delta functions, respectively, defined by

$$\hat{H}(x) = \begin{cases} 1, & x \geqslant 0, \\ 0, & x < 0 \end{cases} \tag{24}$$

and

$$\delta(x) = \frac{\mathrm{d}}{\mathrm{d}x}\hat{H}(x). \tag{25}$$

Consider a two-dimensional level set function ϕ. We employ the level set method for the implicit representation of boundaries. At arbitrary time, the level set model describes a surface in implicit form at zero level as the iso-surface of a scalar function $\phi : R^2 \to R$ embedded in three-dimensional space, as

$$S = \{\mathbf{x} : \phi(\mathbf{x}, 0) = k\}, \tag{26}$$

where k and $\mathbf{x}$ are an arbitrary iso-value and a point on the iso-surface ϕ, respectively. At arbitrary time τ, the surface is represented as

$$S_\tau = \{\mathbf{x}_\tau : \phi(\mathbf{x}_\tau, \tau) = k\}. \tag{27}$$

Using the expressions in Eq. (18) and taking the material derivative of level set function with respect to the parameter τ leads to the "Hamilton–Jacobi equation" as

$$\frac{\mathrm{D}\phi}{\mathrm{D}\tau} \equiv \left.\frac{\partial\phi(\mathbf{x}_\tau, \tau)}{\partial\tau}\right|_{\tau=0} + \nabla\phi(\mathbf{x}_\tau, \tau)|_{\tau=0} \cdot \left.\frac{\mathrm{d}\mathbf{x}_\tau}{\mathrm{d}\tau}\right|_{\tau=0} = \frac{\partial\phi(\mathbf{x}, 0)}{\partial\tau} + \nabla\phi(\mathbf{x}, 0) \cdot \frac{\mathrm{d}\mathbf{x}}{\mathrm{d}\tau} = 0. \tag{28}$$

Note that the transportation of level set function ϕ is defined in the Lagrangian frame whereas the variation of ϕ is done in the Eulerian frame. The mapping between two level set models, i.e. $T(\mathbf{x}, \tau) : \mathbf{x} \to \mathbf{x}_\tau(\mathbf{x})$, $\mathbf{x} \in \Omega$, yields the design velocity field for the shape optimization as

$$\mathbf{x}_\tau \equiv T(\mathbf{x}, \tau) = \mathbf{x} + \tau\mathbf{V}(\mathbf{x}, 0) + \cdots \tag{29}$$

and

$$\frac{\mathrm{d}\mathbf{x}}{\mathrm{d}\tau} \equiv \lim_{\tau\to 0} \frac{\mathbf{x}_\tau - \mathbf{x}}{\tau} = \mathbf{V}(\mathbf{x}, 0) = \mathbf{V}(\mathbf{x}). \tag{30}$$

Thus, Eq. (28) is rewritten by

$$\frac{\partial\phi(\mathbf{x}, 0)}{\partial\tau} = -\nabla\phi(\mathbf{x}, 0) \cdot \mathbf{V}(\mathbf{x}). \tag{31}$$

Let V_n be a speed function normal to the boundary. Using Eq. (20), we have

$$V_n = \mathbf{V} \cdot \mathbf{n} = -\mathbf{V}(x) \cdot \frac{\nabla\phi}{|\nabla\phi|}. \tag{32}$$

Substituting Eq. (32) into Eq. (31) and applying appropriate boundary conditions yield the following equations as:

$$\frac{\partial\phi}{\partial\tau} = V_n|\nabla\phi|, \quad \left.\frac{\partial\phi}{\partial n}\right|_{\Gamma_1} = 0. \tag{33}$$

Given a normal velocity field $V_n(\mathbf{x})$, we can update the level set function $\phi(\mathbf{x})$ at each time step by solving Eq. (33) of the first order partial differential equation with initial values. For computational stability, the "Up-wind scheme" (Sethian, 1999) is employed to solve Eq. (33).

$$\phi_{ij}^{n+1} = \phi_{ij}^n + \Delta t[\max\{-(V_n)_{ij}, 0\}\nabla^+ + \min\{-(V_n)_{ij}, 0\}\nabla^-], \tag{34}$$

where

$$\nabla^+ = \{\max(D_{ij}^{-x},0)^2 + \min(D_{ij}^{+x},0)^2 + \max(D_{ij}^{-y},0)^2 + \min(D_{ij}^{+y},0)^2\}^{\frac{1}{2}} \tag{35}$$

and

$$\nabla^- = \{\max(D_{ij}^{+x},0)^2 + \min(D_{ij}^{-x},0)^2 + \max(D_{ij}^{+y},0)^2 + \min(D_{ij}^{-y},0)^2\}^{\frac{1}{2}}. \tag{36}$$

$D_{ij}^{\pm x}$, $D_{ij}^{\pm y}$, and Δt are the forward and backward difference operators on ϕ_{ij}^n and a time step, respectively. Embedding the obtained level set function ϕ into Eq. (15), the variational problem can be written as

$$\text{Find } e \in Z \text{ such that } a_\phi(e,\bar{e}) = \ell_\phi(\bar{e}) \quad \text{for all } \bar{e} \in \overline{Z}. \tag{37}$$

The bilinear and linear forms are expressed, respectively, as

$$a_\phi(e,\bar{e}) \equiv \int_{\Omega_I} \hat{H}(\phi)\left(\frac{c_g^2}{\eta\omega}\nabla e\cdot\nabla\bar{e} + \eta\omega e\bar{e}\right)\mathrm{d}\Omega \tag{38}$$

and

$$\ell_\phi(\bar{e}) \equiv \int_{\Omega_I} \hat{H}(\phi)\pi\bar{e}\,\mathrm{d}\Omega - \int_{\Omega_I}\delta(\phi)|\nabla\phi|q\bar{e}\,\mathrm{d}\Omega. \tag{39}$$

4. Topological shape optimization

4.1. Formulation of topological shape optimization

The objective of topological shape optimization is to find an optimal layout that minimizes the generalized compliance $\Pi_\phi(e)$ of the system under prescribed loadings. The topological shape optimization problem is stated as

$$\text{Minimize} \quad \Pi_\phi(e) \equiv \int_{\Omega_I}\hat{H}(\phi)\pi e\,\mathrm{d}\Omega - \int_{\Omega_I}\delta(\phi)|\nabla\phi|qe\,\mathrm{d}\Omega, \tag{40}$$

$$\text{Subject to} \quad \int_{\Omega_I}\hat{H}(\phi)\,\mathrm{d}\Omega \leqslant M_{\max}, \tag{41}$$

where $M_{\max}$ is an allowable volume. The function ϕ, playing a role of the design variable and representing the current implicit boundary, is varying as

$$\phi_\tau = \phi + \tau\varphi, \quad \varphi \in \Psi, \tag{42}$$

where φ indicates the direction of boundary variations and belongs to the function space Ψ.

$$\Psi = \{\varphi \in C^1(\Omega_I) : \ \varphi = 0 \text{ on } \Gamma_I^e\}. \tag{43}$$

4.2. Adjoint design sensitivity analysis

Take Fréchet derivative of Eq. (37) with respect to τ in the direction of φ as

$$a_\phi(e',\bar{e}) = \ell'_\phi(\bar{e}) - a'_\phi(e,\bar{e}) \quad \text{for all } \bar{e} \in \overline{Z}, \tag{44}$$

where

$$a'_\phi(e,\bar{e}) \equiv \int_{\Omega_I}\delta(\phi)\left(\frac{c_g^2}{\eta\omega}\nabla e\cdot\nabla\bar{e} + \eta\omega e\bar{e}\right)\varphi\,\mathrm{d}\Omega \tag{45}$$

and

$$\ell'_\phi(\bar{e}) \equiv \int_{\Omega_I} \delta(\phi)\pi\bar{e}\varphi \,\mathrm{d}\Omega - \int_{\Omega_I} \left\{ \delta'(\phi)|\nabla\phi|\varphi + \delta(\phi)\frac{(\nabla\phi)_j(\nabla\varphi)_j}{|\nabla\phi|} \right\} q\bar{e}\,\mathrm{d}\Omega$$
$$= \int_{\Omega_I} \delta(\phi)\left[\pi\bar{e} + \nabla\cdot\left\{q\bar{e}\frac{\nabla\phi}{|\nabla\phi|}\right\}\right]\varphi\,\mathrm{d}\Omega + \int_{\Gamma_I}\delta(\phi)q\bar{e}\frac{\nabla\phi}{|\nabla\phi|}\cdot n\varphi\,\mathrm{d}\Gamma$$
$$= \int_{\Omega_I}\delta(\phi)[\pi\bar{e} - \nabla\{q\bar{e}\}\cdot n - \kappa\{q\bar{e}\}]\varphi\,\mathrm{d}\Omega - \int_{\Gamma_I}\delta(\phi)q\bar{e}\varphi\,\mathrm{d}\Gamma. \tag{46}$$

Consider a generalized compliance functional shown in Eq. (40). Then, we come up with the sensitivity of the generalized compliance, taking advantage of Eq. (46) as

$$\frac{\mathrm{d}\Pi_\phi(e)}{\mathrm{d}\tau} = \int_{\Omega_I}\hat{H}(\phi)\pi e'\,\mathrm{d}\Omega - \int_{\Omega_I}\delta(\phi)|\nabla\phi|qe'\,\mathrm{d}\Omega + \int_{\Omega_I}\delta(\phi)[\pi e - \nabla\{qe\}\cdot n - \kappa\{qe\}]\varphi\,\mathrm{d}\Omega$$
$$- \int_{\Gamma_I}\delta(\phi)qe\varphi\,\mathrm{d}\Gamma. \tag{47}$$

Define an adjoint equation for the power flow problems. Since $e' \in \overline{Z}$, regarding the implicit dependence terms on the design variations as an adjoint load, the adjoint equation is formulated as

$$a_\phi(\lambda,\bar{\lambda}) = \int_{\Omega_I}\hat{H}(\phi)\pi\bar{\lambda}\,\mathrm{d}\Omega - \int_{\Omega_I}\delta(\phi)|\nabla\phi|q\bar{\lambda}\,\mathrm{d}\Omega \quad \text{for all } \bar{\lambda}\in\overline{Z}. \tag{48}$$

Since $e' \in \overline{Z}$, Eq. (48) can be rewritten as

$$a_\phi(\lambda,e') = \int_{\Omega_I}\hat{H}(\phi)\pi e'\,\mathrm{d}\Omega - \int_{\Omega_I}\delta(\phi)|\nabla\phi|qe'\,\mathrm{d}\Omega \quad \text{for all } e'\in\overline{Z}. \tag{49}$$

Also, since $\lambda \in \overline{Z}$, Eq. (44) can be rewritten as

$$a_\phi(e',\lambda) = \ell'_\phi(\lambda) - a'_\phi(e,\lambda) \quad \text{for all } \lambda\in\overline{Z}. \tag{50}$$

Since $a_\phi(\bullet,\bullet)$ is a symmetric operator, Eqs. (49) and (50) are equivalent so that the following equation holds:

$$\int_{\Omega_I}\hat{H}(\phi)\pi e'\,\mathrm{d}\Omega - \int_{\Omega_I}\delta(\phi)|\nabla\phi|qe'\,\mathrm{d}\Omega = \ell'_\phi(\lambda) - a'_\phi(e,\lambda). \tag{51}$$

Substituting Eq. (51) into Eq. (47), we have the following expression:

$$\frac{\mathrm{d}\Pi_\phi(e)}{\mathrm{d}\tau} = \ell'_\phi(\lambda) - a'_\phi(e,\lambda) + \int_{\Omega_I}\delta(\phi)[\pi e - \nabla\{qe\}\cdot n - \kappa\{qe\}]\varphi\,\mathrm{d}\Omega - \int_{\Gamma_I}\delta(\phi)qe\varphi\,\mathrm{d}\Gamma$$
$$= \int_{\Omega_I}\delta(\phi)[\pi\lambda - \nabla\{q\lambda\}\cdot n - \kappa\{q\lambda\}]\varphi\,\mathrm{d}\Omega - \int_{\Gamma_I}\delta(\phi)q\lambda\varphi\,\mathrm{d}\Gamma - \int_{\Omega_I}\delta(\phi)\left(\frac{c_g^2}{\eta\omega}\nabla e\cdot\nabla\lambda + \eta\omega e\lambda\right)\varphi\,\mathrm{d}\Omega$$
$$+ \int_{\Omega_I}\delta(\phi)[\pi e - \nabla\{qe\}\cdot n - \kappa\{qe\}]\varphi\,\mathrm{d}\Omega - \int_{\Gamma_I}\delta(\phi)qe\varphi\,\mathrm{d}\Gamma$$
$$= \int_{\Omega_I}\delta(\phi)\left[\pi(e+\lambda) - \nabla\{q(e+\lambda)\}\cdot n - \kappa q(e+\lambda) - \left(\frac{c_g^2}{\eta\omega}\nabla e\cdot\nabla\lambda + \eta\omega e\lambda\right)\right]\varphi\,\mathrm{d}\Omega$$
$$+ \int_{\Gamma_I}\delta(\phi)q(e+\lambda)\varphi\,\mathrm{d}\Gamma = \int_{\Omega_I}\delta(\phi)\Xi_\phi(e,\lambda)\varphi\,\mathrm{d}\Omega + \int_{\Gamma_I}\delta(\phi)q(e+\lambda)\varphi\,\mathrm{d}\Gamma. \tag{52}$$

Since the following holds,

$$\delta(\phi(x)) = 0 \quad \text{for some } x \notin \Gamma_{\mathrm{I}} \tag{53}$$

and

$$\varphi \equiv \frac{\partial \phi}{\partial \tau} = \frac{\partial \phi}{\partial n}\frac{\partial n}{\partial \tau} = 0 \quad \text{for the other } x \in \Gamma_I. \tag{54}$$

Eq. (52) can be rewritten as

$$\frac{\mathrm{d}\Pi_\phi(e)}{\mathrm{d}\tau} = \int_{\Omega_{\mathrm{I}}} \delta(\phi)\Xi_\phi(e,\lambda)\varphi \,\mathrm{d}\Omega. \tag{55}$$

Next, consider the constraint of allowable material volume as

$$m(\phi) \equiv \int_{\Omega_{\mathrm{I}}} \hat{H}(\phi)\,\mathrm{d}\Omega. \tag{56}$$

Its derivative with respect to the boundary variation is derived as

$$\frac{\mathrm{d}m(\phi)}{\mathrm{d}\tau} = \int_{\Omega_{\mathrm{I}}} \delta(\phi)\varphi \,\mathrm{d}\Omega. \tag{57}$$

4.3. Optimality conditions

The velocity field $V_n(x)$ defines the propagation speed of all level sets of the embedding function $\phi(\mathbf{x})$ along the outward normal direction. The velocity should be determined such that it reduces the generalized compliance of the system while satisfying the requirement of allowable material volume. Define a Lagrangian function Λ for the constrained optimization problems as

$$\begin{aligned}\Lambda(\phi,\mu,s) &= \Pi_\phi(e) + \mu\{m(\phi) + s^2 - M_{\max}\} \\ &= \int_{\Omega_{\mathrm{I}}} \hat{H}(\phi)\pi e \,\mathrm{d}\Omega - \int_{\Omega_{\mathrm{I}}} \delta(\phi)|\nabla\phi| q e \,\mathrm{d}\Omega + \mu\left\{\int_{\Omega_{\mathrm{I}}} \hat{H}(\phi)\,\mathrm{d}\Omega + s^2 - M_{\max}\right\},\end{aligned} \tag{58}$$

where $M_{\max}$, s, and μ are the allowable material volume, a slack variable to convert the inequality constraint to the equality one, and a Lagrange multiplier, respectively. Applying the Kuhn–Tucker optimality conditions leads to

$$\text{(i)}\quad \frac{\mathrm{d}\Lambda(\phi,\mu,s)}{\mathrm{d}\tau} = \frac{\mathrm{d}\Pi_\phi(e)}{\mathrm{d}\tau} + \mu\frac{\mathrm{d}m(\phi)}{\mathrm{d}\tau} = \int_{\Omega_{\mathrm{I}}} \delta(\phi)\{\Xi_\phi(e,\lambda) + \mu\}\varphi \,\mathrm{d}\Omega = 0, \tag{59}$$

$$\text{(ii)}\quad \frac{\mathrm{d}\Lambda(\phi,\mu,s)}{\mathrm{d}\mu} = \int_{\Omega_{\mathrm{I}}} \hat{H}(\phi)\,\mathrm{d}\Omega + s^2 - M_{\max} = 0, \tag{60}$$

$$\text{(iii)}\quad \frac{\mathrm{d}\Lambda(\phi,\mu,s)}{\mathrm{d}s} = 2\mu s = 0, \tag{61}$$

$$\text{(iv)}\quad \mu \geqslant 0. \tag{62}$$

Let

$$\xi = \begin{cases} 0 & \text{if } \int_{\Omega_{\mathrm{I}}} \hat{H}(\phi)\,\mathrm{d}\Omega < M_{\max}, \\ \mu & \text{if } \int_{\Omega_{\mathrm{I}}} \hat{H}(\phi)\,\mathrm{d}\Omega \geqslant M_{\max}, \end{cases} \quad \mu \geqslant 0 \tag{63}$$

the optimality conditions of Eqs. (59)–(62) are then reduced to

$$\frac{\mathrm{d}\Lambda(\phi,\mu,s)}{\mathrm{d}\tau}=\int_{\Omega_\mathrm{I}}\delta(\phi)\{\Xi_\phi(e,\lambda)+\xi\}\varphi\,\mathrm{d}\Omega=0. \tag{64}$$

4.4. Computation of velocity field

Now that the distance function $\phi(\mathbf{x})$ is normal to the boundary and the only normal velocity has influence on the result of shape optimization (Haug et al., 1986), the domain variation can be expressed, using the normal velocity $V_n(x)$, as

$$\Omega_\tau=(\mathbf{I}d+\tau V_n)(\Omega_\mathrm{I}). \tag{65}$$

Using Taylor series expansion in the normal direction of velocity field, the perturbed Lagrangian function can be expressed as

$$\Lambda(\Omega_\tau)=\Lambda\{(\mathbf{I}d+\tau V_n)(\Omega_\mathrm{I})\}=\Lambda(\Omega_\mathrm{I})+\Lambda'(\Omega_\mathrm{I})(\tau V_n)+\cdots, \tag{66}$$

where the sensitivity of the Lagrangian function is expressed as

$$\Lambda'(\Omega_\mathrm{I})=\int_{\Omega_\mathrm{I}}\delta(\phi)\{\Xi_\phi(e,\lambda)+\xi\}\varphi\,\mathrm{d}\Omega. \tag{67}$$

If we take the boundary variation in the descent direction of the sensitivity as

$$V_n=-\{\Xi_\phi(e,\lambda)+\xi\}\varphi, \tag{68}$$

then Eq. (66) can be written as

$$\Lambda(\Omega_\tau)=\Lambda(\Omega_\mathrm{I})-\tau\int_{\Omega_\mathrm{I}}\delta(\phi)\{\Xi(e,\lambda)+\xi\}^2\varphi^2\,\mathrm{d}\Omega+\mathrm{O}(\tau^2)+\cdots. \tag{69}$$

Thus, the decrease of generalized compliance functional is guaranteed while satisfying the requirement of allowable material volume.

4.5. Determination of Lagrange multiplier

To determine a positive Lagrange multiplier ξ, which implies the condition of either active or violated volume constraint, presume that the constraint is active.

$$\int_{\Omega_\mathrm{I}}\hat{H}(\phi)\,\mathrm{d}\Omega=M_{\max}. \tag{70}$$

Taking derivative of Eq. (70) with respect to τ and using Eqs. (33) and (68), the following holds.

$$\int_{\Omega_\mathrm{I}}\delta(\phi)|\nabla\phi|V_n(x)\,\mathrm{d}\Omega=-\int_{\Omega_\mathrm{I}}\delta(\phi)|\nabla\phi|\{\Xi_\phi(e,\lambda)+\xi\}\varphi\,\mathrm{d}\Omega=0. \tag{71}$$

Thus, the Lagrange multiplier is determined by

$$\xi=-\frac{\int_{\Omega_\mathrm{I}}\delta(\phi)|\nabla\phi|\Xi_\phi(e,\lambda)\varphi\,\mathrm{d}\Omega}{\int_{\Omega_\mathrm{I}}\delta(\phi)|\nabla\phi|\varphi\,\mathrm{d}\Omega}. \tag{72}$$

The series of embedding the function $\phi(x)$ generated by the optimization process represent the descent series of the topology optimization problem. This method creates no holes and boundaries. Furthermore, it converges smoothly to a local minimum so that it strongly depends on the initial topology.

5. Numerical examples

In this section, some numerical examples are shown to demonstrate the accuracy of the developed sensitivity analysis method and the applicability of the developed topological shape optimization method. The topology optimization results obtained from the developed level set method are compared with those from the established density method. For the numerical implementation, we use the approximate Heaviside and Dirac-delta functions (as shown in Fig. 3)

$$\hat{H}(x) = \begin{cases} \alpha & \text{if } x < -\Delta, \\ \dfrac{3(1-\alpha)}{4}\left(\dfrac{x}{\Delta} - \dfrac{x^3}{3\Delta^3}\right) + \dfrac{1+\alpha}{2} & \text{if } -\Delta \leqslant x < \Delta, \\ 1 & \text{if } x \geqslant \Delta \end{cases} \tag{73}$$

and

$$\delta(x) = \begin{cases} \dfrac{3(1-\alpha)}{4\Delta}\left(1 - \dfrac{x^2}{\Delta^2}\right) & \text{if } |x| \leqslant \Delta, \\ 0 & \text{if } |x| > \Delta, \end{cases} \tag{74}$$

where α is a small positive number to avoid numerical singularity. Δ is the support length of Heaviside and Dirac-delta functions. Due to the finite length of support in these numerical functions, the domain for the numerical integration is slightly larger than the actual one.

5.1. Example 1: Verification of design sensitivity with respect to boundary variations

The purpose of this example is to verify the accuracy of the derived sensitivity expressions. The model shown in Fig. 4 is 66 mm long, 44 mm wide, and 1 mm thick. The finite element model is composed of 3600 plane elements and 3723 nodes. It is subject to the rate of internal energy generation of 10^7 W/m^2 at the center, the energy flux of 500 W/m at the middle of top and bottom sides, and prescribed energy boundary of 0 J/m^2 at each corner and the middle of left and right sides. The frequency of excitation is 1000 Hz. The following material properties are used: Young's modulus of 195 GPa, Poisson's ratio of 0.28, damping factor of 0.1, material density of 7800 kg/m^3.

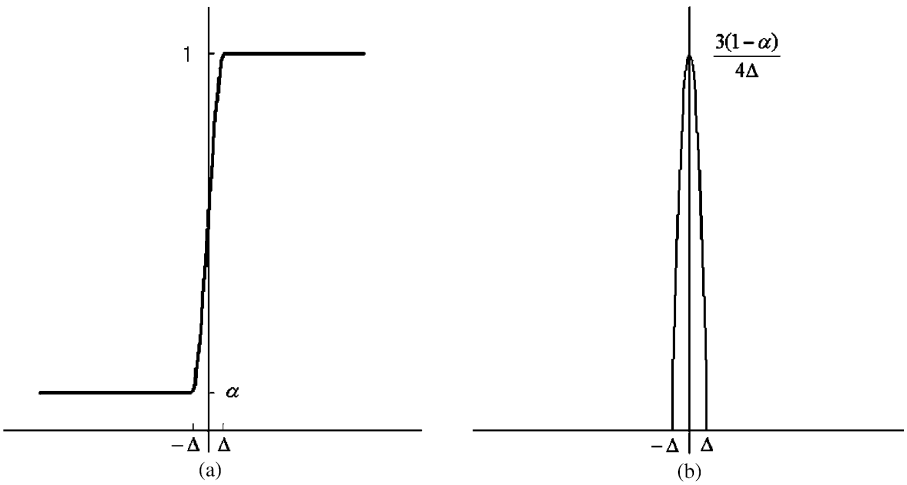

Fig. 3. Approximation of functions: (a) Heaviside function and (b) Dirac-delta function.

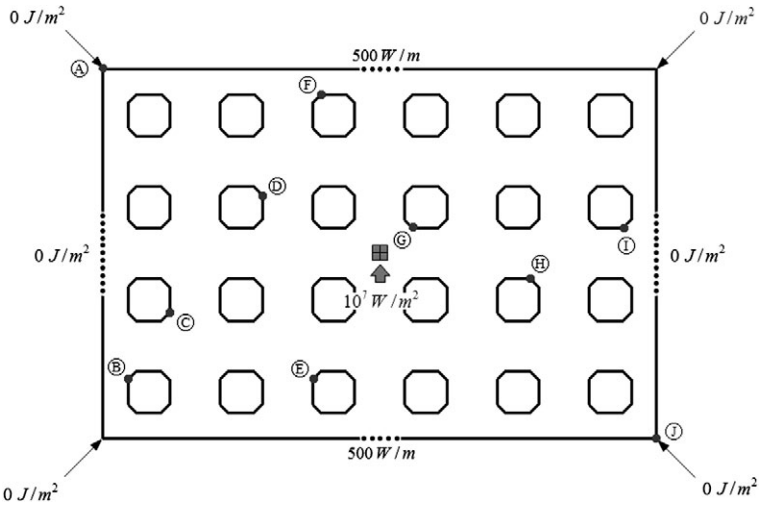

Fig. 4. Model for sensitivity verification.

Table 1
Comparison of generalized compliance sensitivities

	$\frac{d\Pi}{d\tau}$	$\frac{\Delta\Pi}{\Delta\tau}$	$\frac{d\Pi}{d\tau} / \frac{\Delta\Pi}{\Delta\tau} \times 100$		$\frac{d\Pi}{d\tau}$	$\frac{\Delta\Pi}{\Delta\tau}$	$\frac{d\Pi}{d\tau} / \frac{\Delta\Pi}{\Delta\tau} \times 100$
Ⓐ	6.63179E+01	6.60396E+01	100.4214	Ⓕ	9.42135E+00	9.39466E+00	100.2841
Ⓑ	7.54306E−01	7.52042E−01	100.3010	Ⓖ	3.84339E+00	3.83304E+00	100.2701
Ⓒ	6.75008E−01	6.72850E−01	100.3207	Ⓗ	5.11770E+00	5.10376E+00	100.2730
Ⓓ	1.48709E+00	1.48257E+00	100.3045	Ⓘ	7.93957E+00	7.91840E+00	100.2674
Ⓔ	4.73523E−01	4.72007E−01	100.3211	Ⓙ	6.63179E+01	6.60396E+01	100.4214

For the finite difference sensitivity, the boundary is perturbed by 1% of the length of grid used to solve the H–J equation. Arbitrary 10 points on the boundary, Ⓐ through Ⓙ, are selected to compare the analytical sensitivities with finite difference ones. In Table 1, the first and second columns represent the analytical sensitivity obtained from Eq. (55) and the finite difference sensitivity, respectively. The third column represents the percent agreement between the analytical and finite difference sensitivities. At all the points, excellent agreements are observed.

5.2. Example 2: Topological shape optimization (Simply connected topology)

In Fig. 5, the model is subject to the rate of internal energy generation of 10^7 W/m^2 at the center and the prescribed energy boundary of 0 J/m^2 at four corners. Also, the design domain, boundary, and loading conditions are illustrated. A thick line indicates the initial boundary Γ_I. The objective function is to minimize the generalized compliance under the constraint of allowable material volume, 30% of the original one.

In Fig. 6, we compare the optimization histories obtained by applying the level set method to the initial design domain without any holes (a) and with some holes (b) inside the domain. Also, the column (c) shows the optimization history obtained from the established density method. The number in each figure indicates the iteration counter during the optimization process. The density method, with the penalty parameter of 2, yields the optimal material distribution at 241 iterations as shown in (c). As for the level set method, it gives a similar optimal shape to the result obtained from the density method. As the optimization progresses, the

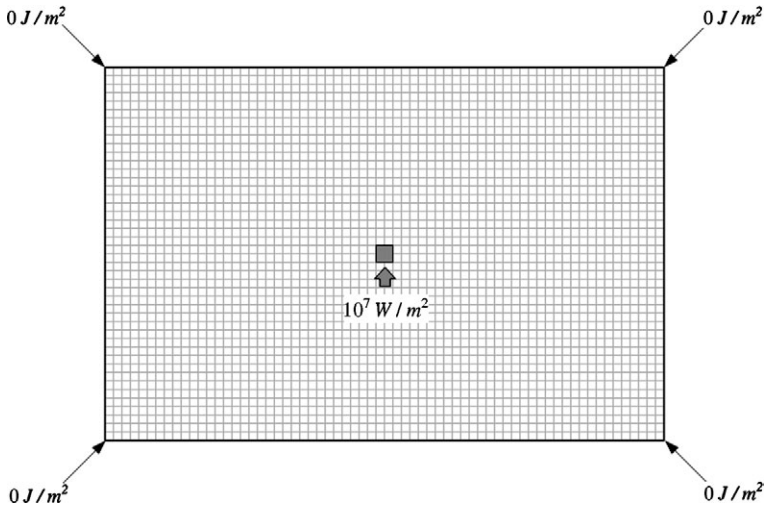

Fig. 5. Design domain and boundary conditions.

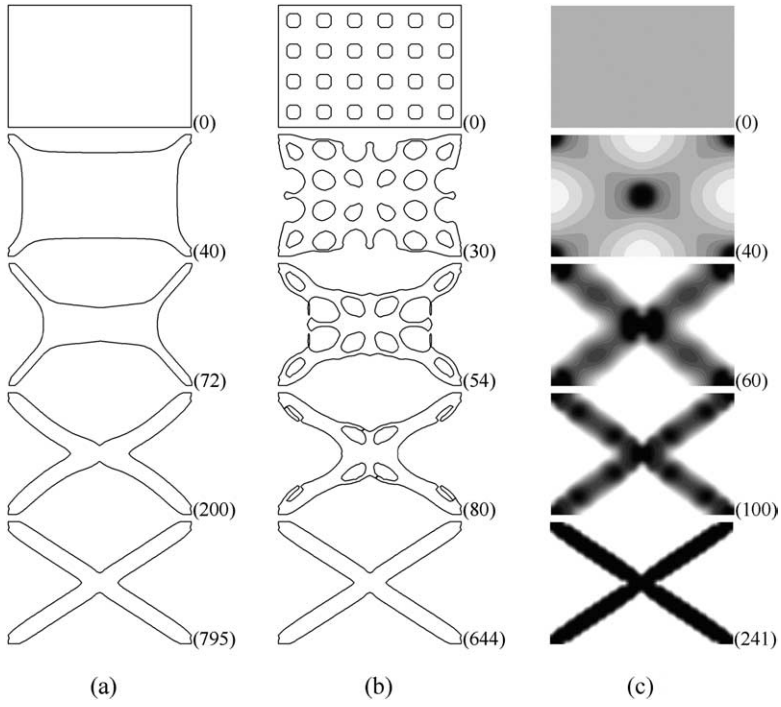

Fig. 6. History of shape changes: (a) level set method (initial domain without holes), (b) level set method (initial domain with holes) and (c) density method.

adjacent holes in (b) are merged one another to finally yield an identical result shown in (a). In this example, the final optimal shape is a simply connected domain so that (a) and (b) give the identical result. Also, they have similar convergence rates but are slower compared with the density method in (c).

Table 2
Comparison of optimization results

	Case (a)	Case (b)	Case (c)
Generalized compliance	5.772	5.766	5.928
Agreement (%)	97.371	97.262	100.000
Number of iterations	795	644	241

In Table 2, the generalized compliance and computing cost are compared. The percent differences of generalized compliance in (a) and (b) with reference to the density method (c) are less than 3%. As for the computing cost, the density method (c) requires the least number of iterations.

Fig. 7 shows optimization histories without initial holes (a), and with initial holes (b). In each case, the volume constraint is satisfied while minimizing the generalized compliance.

In Fig. 8 the design domain, boundary, and loading conditions are illustrated. The plane model is 44 mm long, 44 mm wide, and 1 mm thick. The finite element model for the response analysis is composed of 2500 plane elements and 2601 nodes. It is subject to the rate of internal energy generation of 10^7 W/m^2 at the

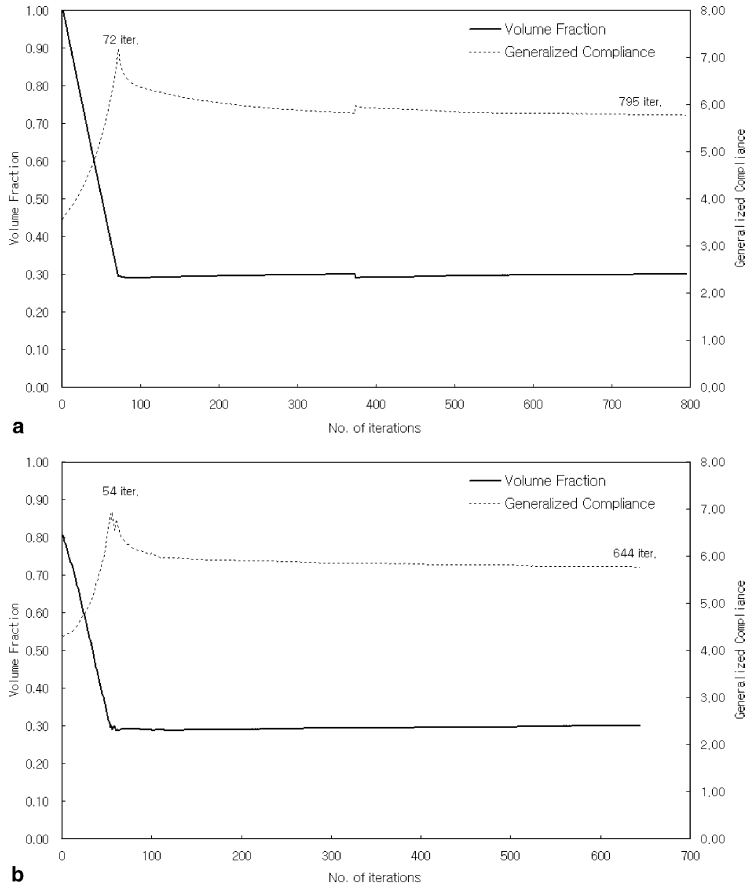

Fig. 7. Optimization histories in level set models (a) and (b).

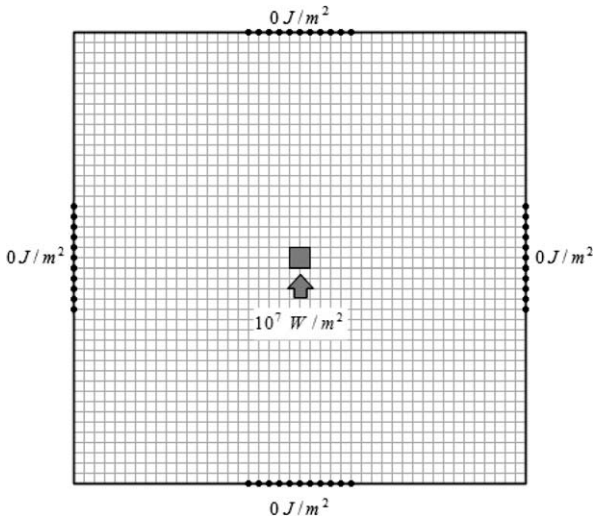

Fig. 8. Design domain and boundary conditions.

center and the prescribed energy boundary of $e = 0$ J/m^2 along four sides. The thick line indicates the initial boundary Γ_I. The objective function is to minimize the generalized compliance under the constraint of allowable material volume whose fraction is 50% of the original one.

Fig. 9 shows the histories of implicit boundaries obtained by applying the level set method to the initial design domain without any holes (a), with some holes (b) inside the domain. The (c) shows the result obtained from the established density method. The density method, with the penalty parameter of 2, yields the optimal material distribution at 126 iterations as shown in (c). As for the level set method, as the optimization progresses, the adjacent holes in (b) are merged to finally yield an identical result shown in (a). In this example, the final optimal shape is also a simply connected domain so that (a) and (b) give an identical result and have similar convergence rates.

Fig. 10 shows optimization history without initial holes (a), and with initial holes (b). In each case, the volume constraint is satisfied while minimizing the generalized compliance. In Table 3, the generalized compliance and computing cost are compared. The percent differences of generalized compliance in (a) and (b) with reference to the density method (c) are less than 2%. As for the computing cost, similarly to the previous example, it takes less computing time with initial holes than without the holes. Thus, we see that the proper initial modeling of the boundary is very important for the efficient computation.

5.3. Example 3: Topological shape optimization (Multiply connected topology)

In Fig. 11, the design domain, boundary, and loading conditions are illustrated. The problem definition is similar to the model shown in Fig. 5, but additional energy flux of 500 W/m is applied at the middle of top and bottom sides. The thick line also indicates the initial boundary Γ_I. The objective is to minimize the generalized compliance under the constraint of allowable material volume whose fraction is 40 % of the original one.

Fig. 12 shows the histories of implicit boundaries obtained by applying the level set method to the initial design domain without any holes (a), with some holes (b) inside the domain. The (c) shows the result obtained from the established density method. The density method, with the penalty parameter of 2, yields the optimal material distribution at 225 iterations as shown in (c). This example shows the importance of the

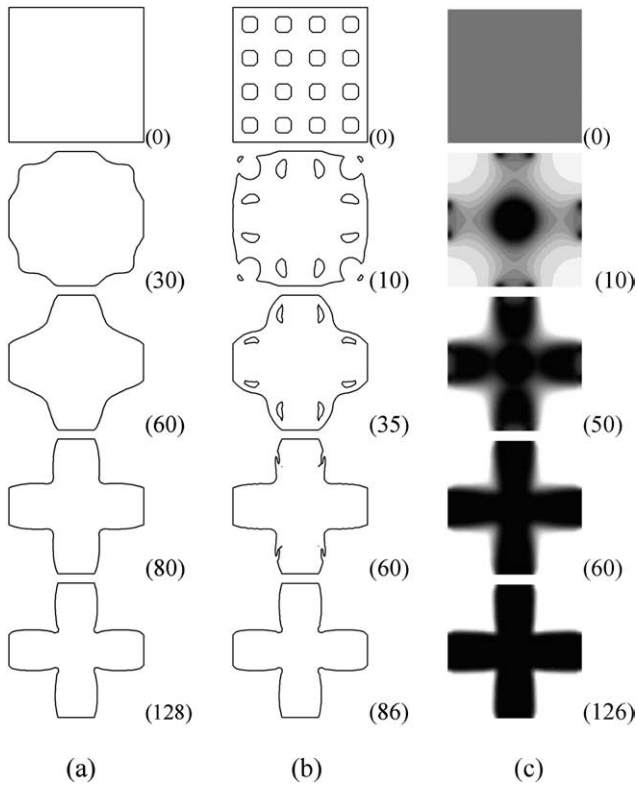

Fig. 9. History of shape changes: (a) level set method (initial domain without holes), (b) level set method (initial domain with holes) and (c) density method.

initial modeling of the boundary. In column (a) and (b), we can see that an initial modeling significantly affects the final shape of boundary. As shown in (c), a density method suggests a multiply connected topological layout. If an initial model has no internal holes, the final optimal shape does not include any internal holes since the developed topology optimization method using the level set method never creates new internal holes. However, the model with initial internal holes can create suitable internal boundary, so the optimal shapes of column (b) and (c) is nearly identical. Thus, we see that the proper initial modeling of the boundary, i.e. the use of sufficient number of holes, is very important for the optimal result. In general, the optimal shape using the level set method is strongly dependent on the initial modeling of the boundary.

Fig. 13 shows the optimization history without initial holes (a), and with initial holes (b). In each case, the volume constraint is satisfied while minimizing the generalized compliance. As for the computing cost, this example requires 405 iterations with initial holes (b) whereas 296 iterations without initial holes (a). However, it is not meaningful to compare both results directly since we obtain different local optima. The density method (c) requires the least number of iterations.

In Table 4, the generalized compliance and computing cost are compared. The percent agreements of generalized compliance in (a) and (b) with reference to the density method (c) are 133% and 97%, respectively. In the case of (a), due to the lack of initial holes, the optimization result is significantly different from the others. Also different generalized compliance is obtained as well. Thus, we notice that the proper initial modeling of the boundary is very important for the optimal result.

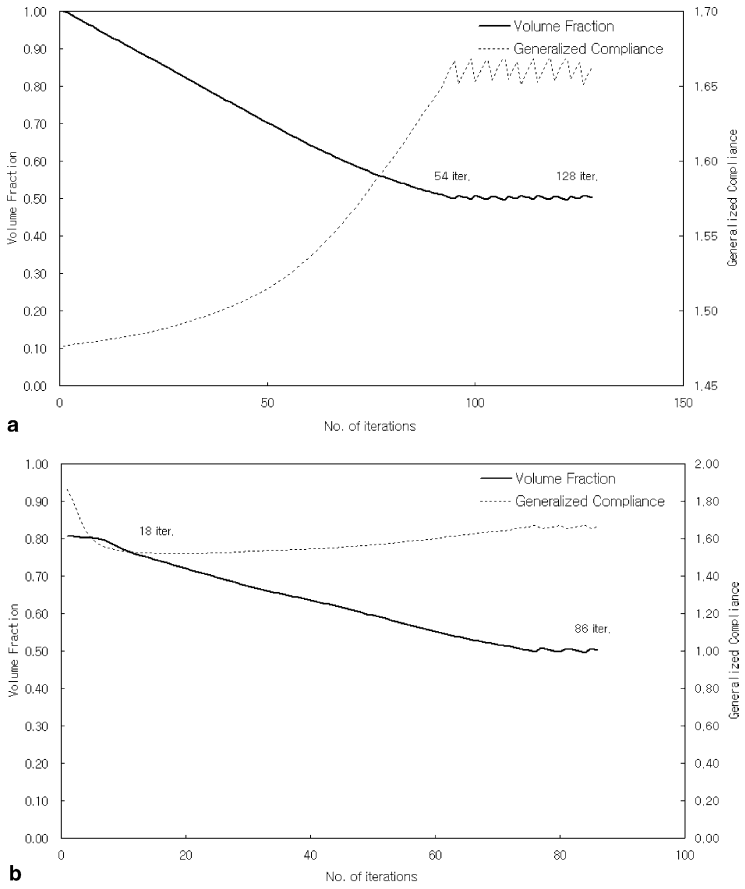

Fig. 10. Optimization histories in level set models (a) and (b).

Table 3
Comparison of optimization results

	Case (a)	Case (b)	Case (c)
Generalized compliance	1.663	1.661	1.686
Agreement (%)	98.620	98.498	100.000
Number of iterations	128	86	126

In this example, the normal velocity field is determined by

$$V_n = -\{\Xi(z,\lambda) + \xi\}\varphi.$$

In Fig. 14, the variation of boundary (a) and the corresponding velocity field (b) are plotted during the optimization. The Fig. 14(b) indicates the magnitude of normal velocity. After convergence, the magnitude of normal velocity vanishes throughout the whole domain except the region where the loading and boundary conditions are applied. This is mainly due to the requirement of function space for the level set function shown in Eqs. (42) and (43) as

$$\phi_\tau = \phi + \tau\varphi, \quad \varphi \in \Psi \text{ where } \Psi = \{\varphi \in C^1(\Omega_I) : \varphi = 0 \text{ on } \Gamma_I^e\}.$$

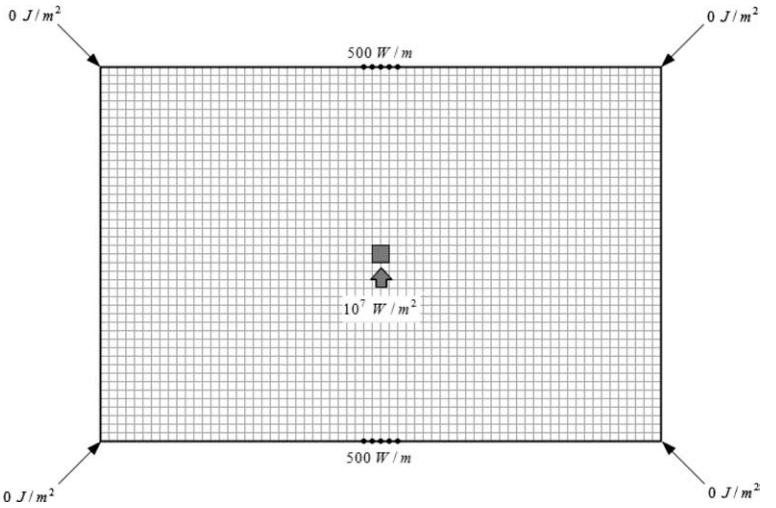

Fig. 11. Design domain and boundary conditions.

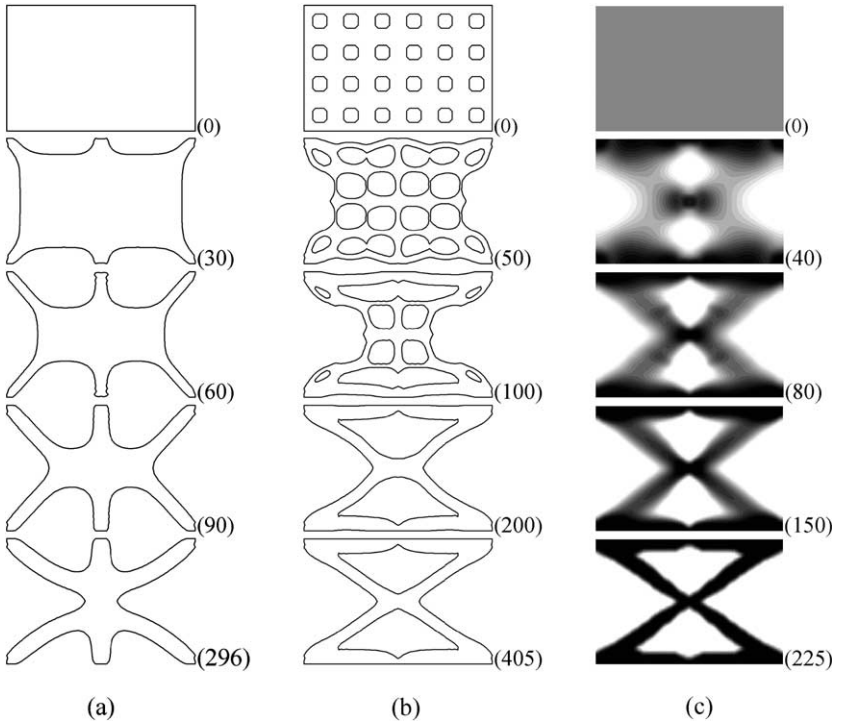

Fig. 12. History of shape changes: (a) level set method (initial domain without holes), (b) level set method (initial domain with holes) and (c) density method.

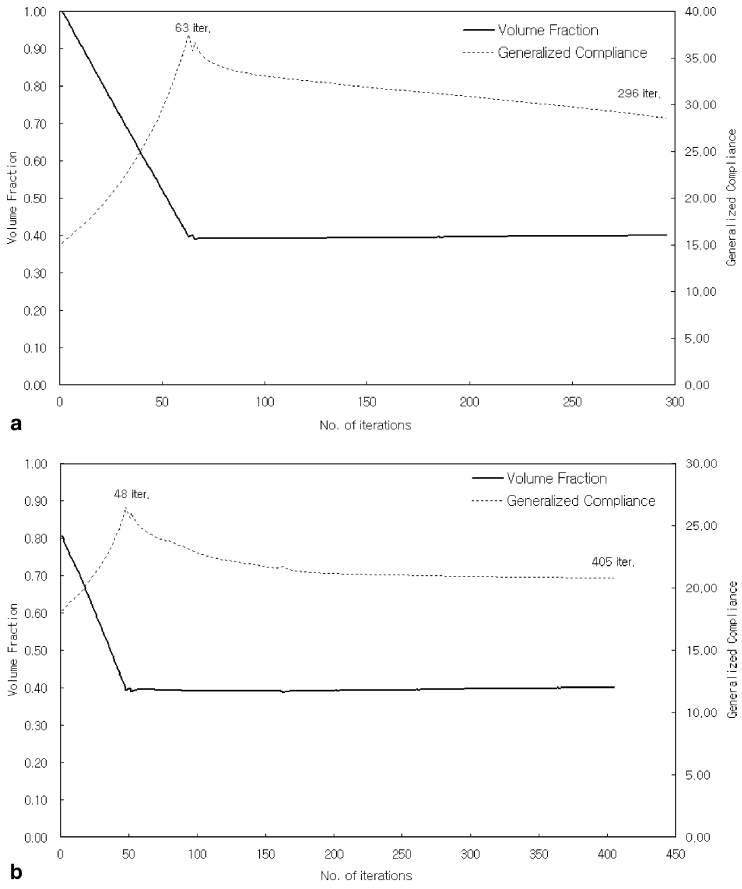

Fig. 13. Optimization histories in level set models (a) and (b).

Table 4
Comparison of optimization results

	Case (a)	Case (b)	Case (c)
Generalized compliance	28.551	20.810	21.493
Agreement (%)	132.838	96.825	100.000
Number of iterations	296	405	225

To investigate the effectiveness of topology optimization method, the distributions of energy density for the original and optimal models are compared. To represent the volume fraction, we introduce a normalized bulk material density function that has a continuous variation from zero to one, taking the value of 1.0 for solid material and 0.0 for void. For the original model, the bulk material density is reduced to 0.4 to represent the volume requirement, the original material volume of 40%. Fig. 15(a) shows the distribution of energy density for the original model that has the bulk material density of 0.4 and Fig. 15(b) for the optimal model. The maximum of energy density is significantly reduced by 21% under the same amount of material volume.

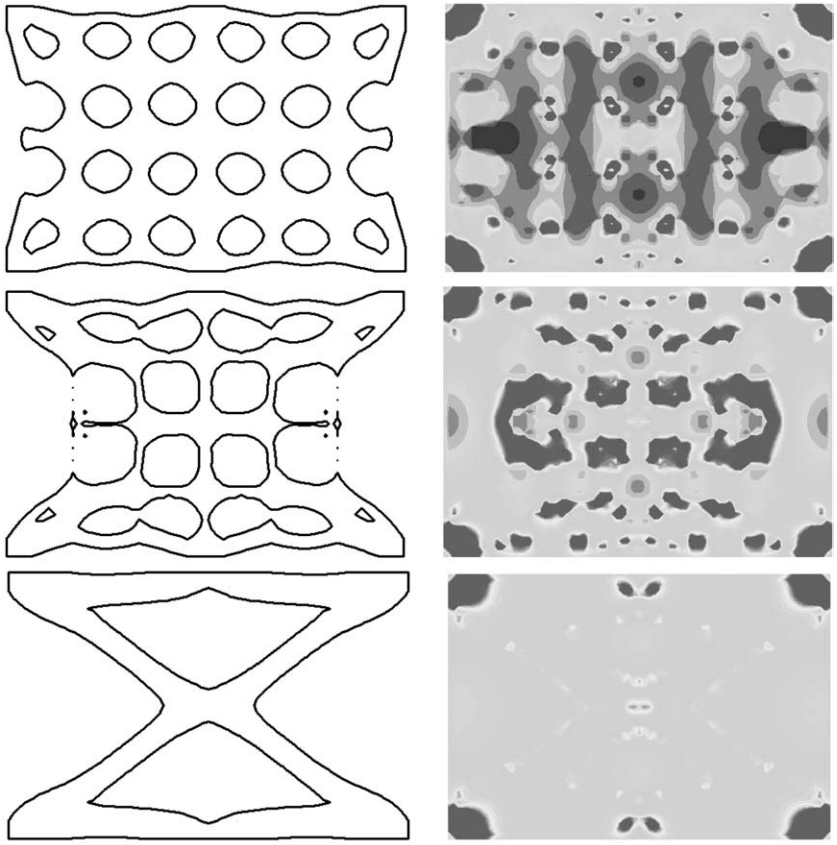

Fig. 14. Boundary and velocity field during optimization: (a) variation of boundary and (b) variation of velocity field.

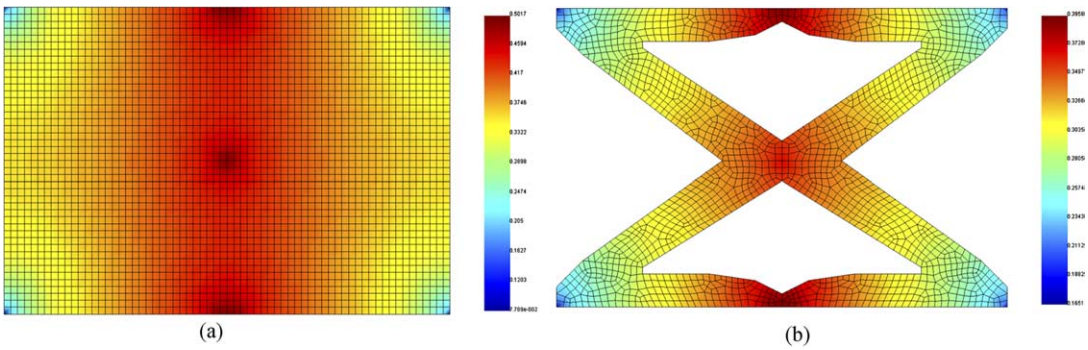

Fig. 15. Distribution of energy density at 1000 Hz: (a) original model (maximum = 0.5017 J/m^2) and (b) optimal model (maximum = 0.3958 J/m^2).

6. Conclusions

A topological shape optimization method for power flow problems in steady state is developed using the level set method. Since the implicit moving boundary is used, it is easy to represent the shape variations and there is no need to re-parameterize after significant shape changes during the optimization. Necessary design gradients are computed very efficiently using the adjoint sensitivity analysis method. The overall computing cost for the topology optimization is moderately expensive compared with the established density method. For the optimization process, the boundary velocity to solve the Hamilton–Jacobi equation is derived from Kuhn–Tucker optimality condition for the Lagrangian function. Some illustrative numerical examples show that the level set method yields the similar optimal shape to the established density approach. Even though the domain experiences significant shape changes, the level set method always gives a smooth boundary. Also, the use of sufficient number of initial holes in the domain is very important to get the reasonable results since this method creates no holes during the optimization.

Acknowledgements

This work was supported by Advanced Ship Engineering Research Center of the Korea Science and Engineering Foundation (Grant Number R11-2002-104-03002-0) in 2003–2004. The support is gratefully acknowledged. Also the authors wish to thank the *Ship Noise and Vibration Laboratory* (*SNOVIL*) in Seoul National University for the helpful discussion and validation of optimization results.

References

Allaire, G., Jouve, F., Toader, A., 2002. A level-set method for shape optimization. Comptes Rendus de L Academie Des Sciences Paris, Serie I 334, 1125–1130.

Belov, V.D., Rybak, S.A., Tartakovskii, B.D., 1977. Propagation of vibrational energy in absorbing structures. Journal of Soviet Physics Acoustics 23 (2), 115–119.

Bendsøe, M.P., 1989. Optimal shape design as a material distribution problem. Structural Optimization 1, 193–202.

Bendsøe, M.P., Kikuchi, N., 1988. Generating optimal topologies in structural design using a homogenization method. Computer Methods in Applied Mechanics and Engineering 71, 197–224.

Butlitskaya, I.A., Vyalyshev, A.I., Tartakovskii, B.D., 1983. Propagation of vibrational and acoustic energy along a structure with losses. Journal of Soviet Physics Acoustics 29 (4), 333–334.

Haug, E.J., Choi, K.K., Komkov, V., 1986. Design Sensitivity Analysis of Structural Systems. Academic Press, New York.

Kim, N.H., Dong, J., Choi, K.K., 2004. Energy flow analysis and design sensitivity analysis of structural problems at high frequencies. Journal of Sound and Vibration 269, 213–250.

Nefske, D.J., Sung, S.H., 1989. Power flow finite element analysis of dynamic systems: basic theory and application to beams. Journal of Vibration, Acoustics, Stress and Reliability in Design 111, 94–100.

Osher, S., Sethian, J.A., 1988. Front propagating with curvature dependent speed: algorithms based on Hamilton–Jacobi formulations. Journal of Computational Physics 79, 12–49.

Sethian, J.A., 1999. Level Set Methods and Fast Marching Methods. Cambridge University Press, Cambridge.

Sethian, J.A., Wiegmann, A., 2000. Structural boundary design via level set and immersed interface methods. Journal of Computational Physics 163, 489–528.

Wang, M.Y., Wang, X., Guo, D., 2003. A level set method for structural topology optimization. Computational Methods in Applied Mechanics and Engineering 192, 227–246.